# Fuel-Assisted Solar Thermal Power Plant with supercritical ORC cycle

# Fuel-Assisted Solar Thermal Power Plant with supercritical ORC cycle

*Fiaschi Daniele [a], Lifshitz Adi[a] , Manfrina Giampaolo [a]*

*[a] Università degli Studi di Firenze, Dipartimento di Energetica "Sergio Stecco"*
*Via C. Lombroso 6/17 – 50135 Firenze - Italy*

**Abstract:** In this paper, a 100 kWe reference size solar thermal power plant is considered, having the following features:
- Use of parabolic trough solar collectors with 1-degree of freedom solar tracking
- Double circuit with a liquid heat transfer fluid, connecting the solar field to a supercritical organic vapour generator
- No heat storage; the unavailability of radiation is met by external firing with a suitable fuel, limiting as far as possible the use of this last
- Supercritical ORC system with regenerator, using different possible organic fluids

The operation of the system is considered over the year; the design conditions are assumed at a radiation level I = 700 W/m$^2$. For lower radiation conditions, external firing is switched on, and the ORC system is operated anyway under design conditions. When radiation is larger, the ORC is operated under off-design conditions, with increased flow rate.
The results confirm that, with a careful choice of the design conditions (type of fluid, pressure, heat exchanger optimization,...) a good performance can be achieved with limited external fuel integration; the performance of the system does not suffer extensively from operation under off-design. An exergy analysis is included examining the contributions of component exergy destructions and system exergy losses over typical daily operations.

**Keywords:** Solar thermal Energy Conversion, Organic Rankine Cycles, Supercritical, Off-design.

## 1. Introduction

Solar thermal power plants are an interesting option for power generation from renewables, and can be competitive with photovoltaic energy conversion systems.

The attractiveness of solar thermal power plants is documented by the technical literature, by the operability demonstrated by the first large-scale pilot plants, and by the existence of extensive projects in the near future [1, 2, 3]. As an alternative to building very large solar thermal power plants, equipped with large heat storage systems (e.g. molten salts), a smaller size installation (100 kWe nominal) is proposed, capable of following the availability of solar radiation; when necessary (for low radiation values) the plant is supported by external firing through an auxiliary heater, which substitutes the expensive and inefficient heat storage system. The small-size power plant can be switched off during the night. The typical application considered is for Middle-East desert locations or African Mediterranean countries, which often have considerable land availability as well as favorable radiation conditions.

## 2. General layout

Figure 1 shows the general layout of the power plant. A typical solar energy generating system (SEGS) arrangement is considered, which has demonstrated durability and availability in large-scale applications [3, 4, 5].

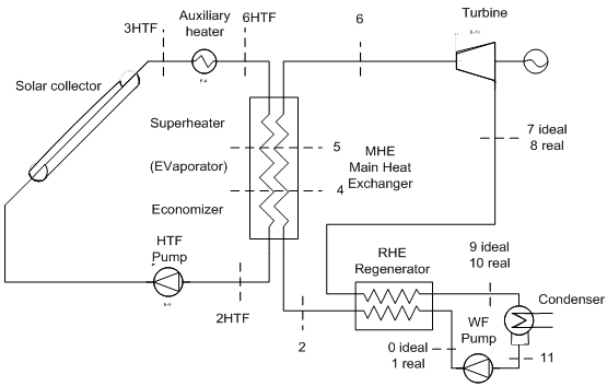


*Fig. 1. Solar Thermal Power Plant Layout*

The plant uses a dual circuit: in the solar field (primary circuit), a high-temperature oil is used as heat transfer fluid HTF [7]; the main heat exchanger MHE links the primary and the secondary circuit. In the latter, an organic vapor is used in place of steam. This choice allows to use reasonable pressures and size of equipment (turbine, condenser) for a small power plant. As many organic fluids have a limit curve with negative slope, the secondary circuit includes a regenerator RHE, which improves cycle performance and reduces the cooling load at the condenser. The primary circuit includes an auxiliary heater: this is fed using a conventional fuel (natural gas or oil, depending on local availability).

## 3. Selection of the Working Fluid

The correct selection of the organic working fluid (WF) to be used in the secondary circuit represents a key issue in low-temperature thermal energy conversion processes [6]. The desired features are:

- The WF should be capable of long-term operation at the design temperature level, which is imposed by current SEGS solar collector technology; it must be safe and compatible with materials used within the power plant
- The WF should be operated at reasonable pressure conditions both at steam generator and condenser
- The possibility of building the plant with a supercritical vapor generator is interesting, because it allows an improved matching of heat capacities between the primary and secondary circuit, in comparison with sub-critical vapor cycles.

The main system parameters are :

- The Heat Transfer Fluid's (HTF) maximum temperature is set to $T_{M\_HTF}$ = 390 °C (Therminol VP-1; base pressure in the primary circuit $p_{HTF}$ = 1500 kPa; specific heat is $c_{pHTF}$ = 2,32 kJ/(kgK)).
- The temperature at the condenser is set to $T_{11}$ = 35 °C.
- The reference values for ambient temperature and direct irradiation were set at $T_{amb}$ = 25 °C and $I_b$ = 700 W/m² .
- The temperature differences at the MHE hot end $DT_{HE}$ and at the entrance to the evaporator $DT_{EE}$ (in case of sub-critical cycle) were set at 20 °C. In the super-critical case the temperature difference was set at 20°C at the same point (where the critical temperature is reached).
- The RHE effectiveness was set at ε = 0,8 (ε = 0,9 in alternative).
- The pump and turbine isentropic efficiencies were set to $\eta_T$ = 0,85 ; $\eta_P$ = 0,85 .

The difference between a sub-critical and a super-critical cycle is shown in Figure 2. In the specific case here considered (Toluene), it is clear that the imposition of a maximum value $T_6$ = 370 °C for the WF temperature determines exit from the turbine (point 8) in highly-superheated conditions. As the critical pressure for Toluene is 4126 kPa, $p_0$ = 5000 kPa was chosen for the supercritical cycle.

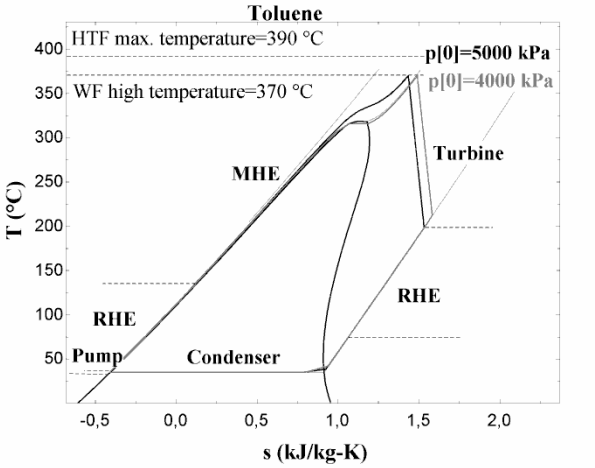


*Fig. 2. Example of subcritical and supercritical cycles*

The working fluids considered are resumed in Tables 1 and 2.

*Table 1. Cycle parameters for different WFs.*

| Working Fluid | $p_0$ kPa | | $DT_{CE}$ °C | $m_{WF}$ kg/s | $m_{HTF}$ kg/s |
|---|---|---|---|---|---|
| Toluene | 5000 | A | 103 | 0,40 | 0,81 |
| Cyclohexane | 6500 | A | 53 | 0,41 | 0,71 |
| n-dodecane | 1000 | B | 107 | 0,4 | 1,44 |
| Ethanol | 8000 | A | 68 | 0,21 | 0,51 |
| n-heptane | 6000 | A | 36 | 0,42 | 0,70 |
| Ammonia | 26000 | A | 24 | 0,18 | 0,422 |
| Steam | 1700 | B | 137 | 0,09 | 0,57 |

A = Supercritical B = Subcritical

The values of $\eta_{TS}$ reported in Table 2 were determined after a search for possible maximum

efficiency conditions with variable cycle pressure $p_0$. The trend of $\eta_c$ in function of $p_0$ is shown in Figure 3. Results shown in Table 2 and in Figure 3 indicate that a supercritical cycle using Toluene is the most recommendable choice under the considered technical constraints. It is also interesting to notice that Toluene implies a reasonable size of the RHE (with a heat duty limited to 77 kW, much smaller than for other WFs here considered).

*Table 2. Cycle performance for different WFs ($\varepsilon$ = 0,8)*

| Working fluid | $Q_{MHE}$ kW | $Q_{RHE}$ kW | $Q_C$ kW | W kW | $p_0$ MPa | $\eta_{TS}$ |
|---|---|---|---|---|---|---|
| Toluene | 282 | 77 | 184 | 98 | 5 | 0,247 |
| Cyclo-hexane | 283 | 116 | 187 | 96 | 6,5 | 0,242 |
| n-dodecane | 278 | 167 | 184 | 94 | 1 | 0,237 |
| Ethanol | 287 | 24 | 196 | 91 | 8 | 0,230 |
| n-heptane | 284 | 153 | 191 | 92 | 6 | 0,234 |
| Ammonia | 289 | 22 | 207 | 82 | 26 | 0,207 |
| Steam | 286 | 0 | 206 | 80 | 1,7 | 0,202 |

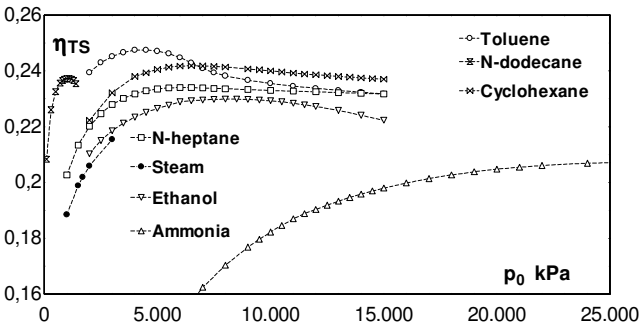


*Fig. 3. Calculated cycle performance for different WFs; sensitivity to pressure conditions ($p_0$)*

The performance of the ORC system is very sensitive to the efficiency of the regenerator. In fact, the RHE heat duties are significant as the end of expansion is well inside the superheated region. The effect of improving ε = 0,9 is shown in Table 3.

## 3. Subcritical vs. supercritical

The advantage of considering a supercritical organic cycle is clear when considering the heat transfer diagram of the MHE. In the subcritical case (Figure 4), it is impossible to improve matching of heat capacities on the hot and cold sides of the MHE: in fact, at least in the evaporator the heat capacity goes to infinity ($c_{p\ WF} = \infty$ with finite flow rate). This determines an uneven temperature profile, with a pinch condition at the end of economizer section (EE), and larger values of $DT_{CE}$ (Table 1); this determines a lower efficiency of the MHE for equal NTU (or surface).

*Table 3. Cycle performance for different WFs ($\varepsilon$ = 0,9)*

| Working fluid (*) | $Q_{MHE}$ kW | $Q_{RHE}$ kW | $Q_C$ kW | W kW | $p_0$ MPa | $\eta_{TS}$ |
|---|---|---|---|---|---|---|
| Toluene | 282 | 98 | 180 | 102 | 4 | 0,257 |
| Toluene | 282 | 90 | 180 | 101 | 5 | 0,256 |
| Cyclohexane | 282 | 145 | 181 | 101 | 5,5 | 0,255 |
| Cyclohexane | 283 | 137 | 182 | 101 | 6,5 | 0,255 |
| n-dodecane | 278 | 203 | 176 | 102 | 1 | 0,256 |
| n-heptane | 283 | 184 | 183 | 99 | 6 | 0,250 |

(*) with respect to Table 2, Ammonia and Ethanol were not considered because of the very low regenerated heat.

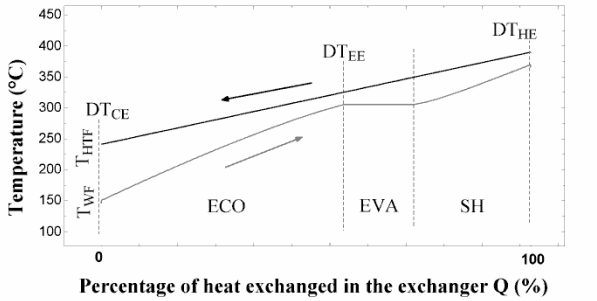


*Fig. 4. Heat Transfer diagram of MHE; subcritical case (Toluene, $p_0$=350 0kPa)*

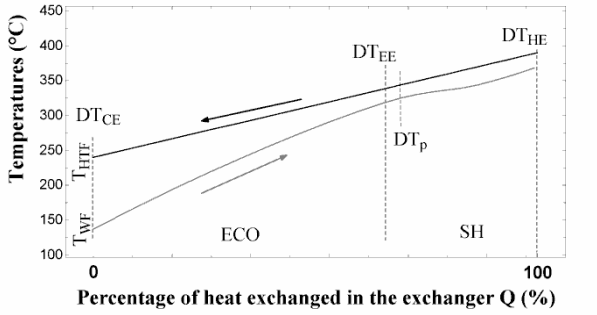


*Fig. 5. Heat Transfer diagram of MHE; supercritical case (Toluene)*

The situation is much improved in supercritical conditions (Figure 5). In this case, the WF heat capacity varies gradually with temperature, so that

a better matching of the heat transfer curve can be obtained (and consequently, lower values of $DT_{CE}$ result – Table 1). Figure 5 also shows that the pinch condition is not necessarily located at the EE point.

## 4. Off-design Operation

When radiation is different from the reference conditions ($I_b$ = 700 W/m$^2$), the system is operating in off-design. In order to limit the deterioration of performance, without recurring to complex heat storage devices, whose transient performance is penalizing, the following guidelines were followed:

A. when radiation $I_b$ < 700 W/m$^2$, the auxiliary burner is switched on, reaching anyway $T_{M\_HTF}$= 390°C; the design flow rate is circulated both in the primary and secondary circuits. Only the solar collector is operating in off-design. The system operates in a fuel-assisted mode (a Solar Fraction SF is defined)

B. when radiation $I_b$ > 700 W/m$^2$, the auxiliary burner is off; the condition $T_{M\_HTF}$= 390°C is not exceeded as the flow rate is augmented both in the primary and secondary circuits. Pressure and temperature conditions are not changed. The whole system is operated in off-(over-) design. The performance level is affected, but extra power is produced.

### 4. 1. Solar collector off-design

The collector performance is modeled through its thermal efficiency curve [5]

$$\eta_{coll} = 0,745 - 0,0065 \cdot X - 0,000339 \cdot I \cdot X^2 \quad (1)$$

Where:

$$X = \frac{T_{abs} - T_{amb}}{I_b} \quad (2)$$

$$T_{abs} = \frac{T_{2HTF} + T_{3HTF}}{2} \quad (3)$$

The collectors are placed horizontally on the ground, with a daily East-West tracking system operating at a nominal rate of 15 degrees per hour.

### 4. 2. Low-radiation system off-design

Figure 6 summarizes the off-design performance of the collector and the reflected effects on the overall system performance, for case (A), $I_b$ < 700 W/m$^2$; it can be seen that $\eta_{Coll}$ is affected by low radiation conditions; the efficiency of the auxiliary heater was assumed constant at $\eta_{aux}$ = 0,9.

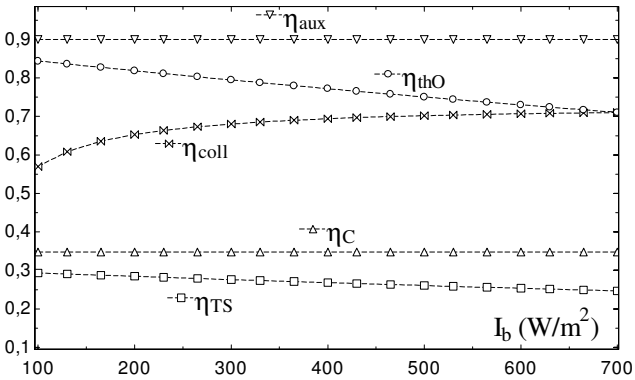


*Fig. 6. System efficiencies with variable radiation ($I_b$ < 700 W/m$^2$)*

The overall thermal (collector/auxiliary heater/MHE) system efficiency is defined as the ratio of the heat transferred to the WF in the MHE, divided by the overall heat input to the system:

$$\eta_{thO} = \frac{Q_{MHE}}{Q_{aux} + \frac{A_u \cdot I_b}{1000}} \quad (4)$$

$\eta_{thO}$ decreases with increasing radiation: in fact, $\eta_{aux}$ = 0,9 is always much larger than $\eta_{coll}$, so that from a purely energetic point of view it is preferable to operate the system on fuel rather than on solar radiation. The power cycle in case (A) is the same as in the 'design' state (pressure, temperature and flow rates in the secondary circuit), and so the power cycle efficiency remains constant for I< 700 W/m$^2$.

The total system efficiency $\eta_{TS}$ is the product of the Overall Thermal efficiency $\eta_{thO}$ and of the conversion efficiency $\eta_c$, and so it decreases with increasing radiation and increasing external firing.

### 4. 3. High-radiation system off-design

When $I_b$ > 700 W/m$^2$, the auxiliary heater is switched off; the heat transferred in the MHE is equal to that captured by the collector; therefore $\eta_{thO}$ is equal to $\eta_{coll}$ - which depends on radiation according to Eqs. 1-3.

The control law for flow rate (primary circuit) maintains the HTF temperature at the outlet of the solar field to its maximum value, $T_{M\_HTF}$= 390°C; the approach value at the hot end of the heat exchanger $DT_{HE}$ was maintained at 20 °C; the WF temperature at turbine inlet is then fixed at $T_6$ = 370 ºC, and the flow rate in the secondary circuit is consequently adjusted. In order to do that, it is necessary to re-evaluate the performance of heat exchangers (MHE and RHE) under the new, off-design condition with increased flow rates.

The heat balance of the heat exchanger [1] is resumed by the following equations:

$$Q_{MHE} = m_{HTF} \cdot c_{pHTF} \cdot (T_{3HTF} - T_{2HTF}) = m_{WF} \cdot (h_6 - h_2) \quad (5)$$

$$Q_{MHE} = U \cdot A \cdot DT_{LM} \quad (6)$$

$$DT_{LM} = \frac{(T_{3HTF} - T_6) - (T_{2HTF} - T_2)}{\ln \frac{(T_{3HTF} - T_6)}{(T_{2HTF} - T_2)}} \quad (7)$$

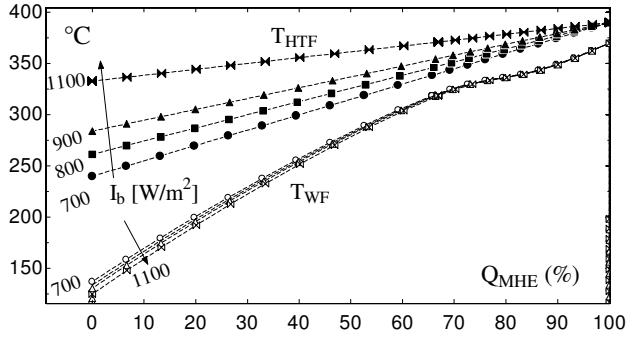


*Fig. 7. MHE heat transfer diagram at off-design ($I_b$ > 700 W/m²)*

As a first approximation, a constant global heat transfer coefficient U was assumed. This assumption is precautionary since actually U increases as the mass flow rate increases [8]. As A is fixed, the increase in $Q_{MHE}$ is thus directly reflected by an increase in $DT_{LM}$; as the temperature conditions on the cold side (WF; $T_6$, $T_2$) are not changed[2] as well as the condition at collector outlet ($T_{3HTF}$), this is obtained decreasing the value of $T_{2HTF}$; in turn, this affects the collector performance (Equation 3); an NTU-ε correlation method (counter-flow heat exchanger) was used to close the system of equations (MHE and RHE) at off-design. The resulting increase in the temperature difference at the cold end is shown in Figure 7.

### 4. 4. Generalized system off-design

Considering operation over the full range of radiation, the relevant circuit temperatures are shown in Figure 8, and the flow rate values in Figure 9.

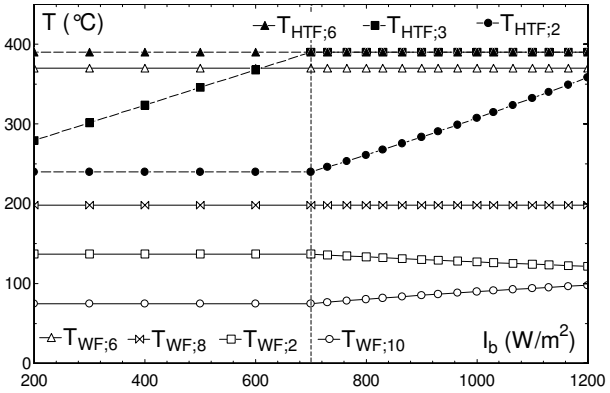


*Fig. 8. Circuit temperatures at off-design*

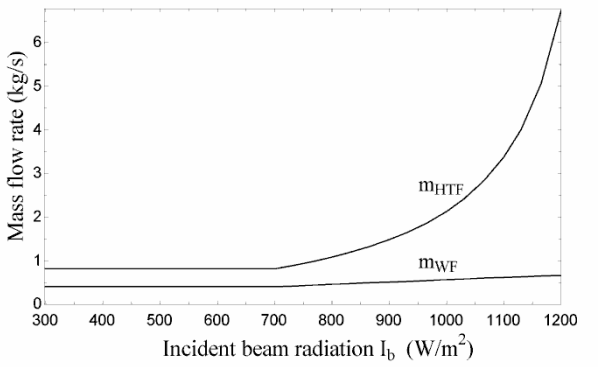


*Fig. 9. Circuit flow rates at off-design*

The temperature rise of the WF in the MHE remains relatively constant as the radiation increases; accordingly, $m_{WF}$ increases proportionally to $Q_{MHE}$. On the other hand, the temperature difference of the HTF in the primary side of the MHE decreases greatly due to the increase of the LMTD in the exchanger, as discussed before; this produces an augmented HTF mass flow rate (Figure 9). A too large increase in $m_{HTF}$ is not desirable, since it would produce large

[1] Here, the MHE; a similar procedure is followed for the RHE.

[2] $T_2$ changes slightly with RHE effectiveness

pressure losses in the solar-field primary circuit. However, it is important to notice that in reality $m_{HTF}$ exceeds 2 kg/s only when $I_b$ >1000 W/m$^2$, which is a condition very seldom reached even at the desert climate design location.

The augmented mass flow rate $m_{WF}$ for $I_b$ > 700 W/m$^2$ determines also for the RHE an increase of $DT_{ML}$; consequently the regenerator's effectiveness is slightly decreased; also $Q_{RHE}$ is decreased with respect to design, and more heat must be rejected to the environment in the condenser. This has a marginally negative effect on the cycle efficiency $\eta_C$ (Figure 10).

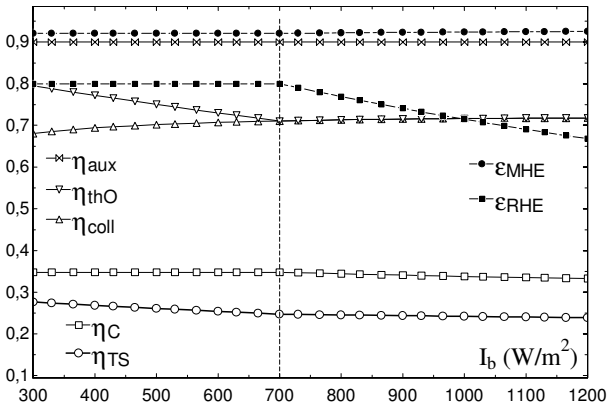


*Fig. 10. System efficiencies and RHE effectiveness at off-design*

## 5. Daily and Seasonal Models

Having determined the system settings and performance at design conditions, and developed a simplified model for off-design, it is possible to calculate short- (daily) or long-term (seasonal) performance.

The Solar Fraction of the energy conversion system over a certain time period can be expressed by:

$$SF = \frac{\int_0^T Q_{coll}\,dt}{\int_0^T Q_{coll}\,dt + \int_0^T Q_{aux}\,dt} \quad . \qquad (8)$$

The higher is the value of $I_{bD}$, the more the system will work with auxiliary heating switched on, resulting in a lower overall SF. A low value of $I_{bD}$, however, results in the system working for long periods at $I_b$ > $I_{bD}$ "off-design" conditions, hence with a reduced overall conversion efficiency and lower overall energy production. Therefore, the choice of $I_{bD}$ is a compromise between high SF and high system efficiency.

As a first example, the daily operation of the system was simulated on July 8$^{th}$ (a clear sunny day) and 17$^{th}$ (a day with relevant intermittency of solar radiation). The radiation data and the calculated performance are reported in Figures 11 and 12. The Overload is defined as $m_{WF}/m_{WF,D}$*100.

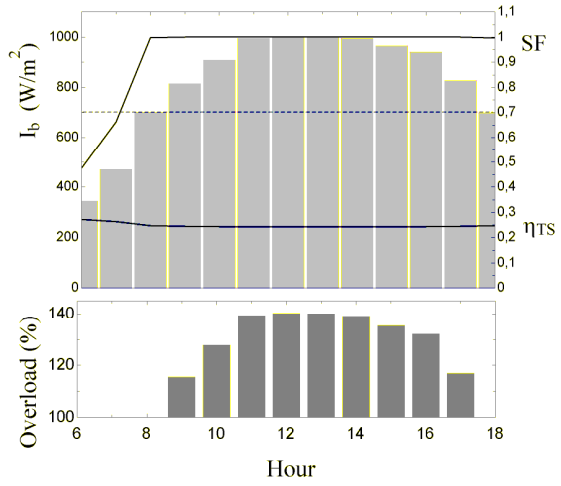


*Fig. 11. Daily radiation and ambient temperature (Sede-Boqer, Negev desert; July 8$^{th}$)*

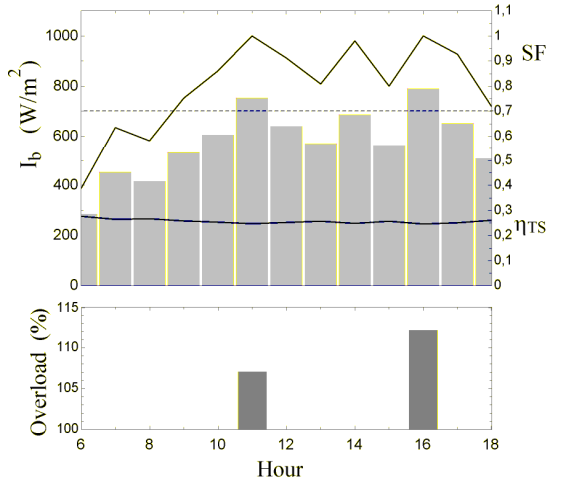


*Fig. 12. Daily radiation and calculated performance (Sede-Boqer, Negev desert; July 17$^{th}$)*

In order to show the situation for winter operation, the same data are reported in Figure 13 for January 10$^{th}$ (in this day radiation was always low, so that the plant was run at 100% power using auxiliary firing).

The daily-averaged situation is resumed for some reference days in Table 4. A monthly simulation

was also performed. The results are summarized in Table 5.

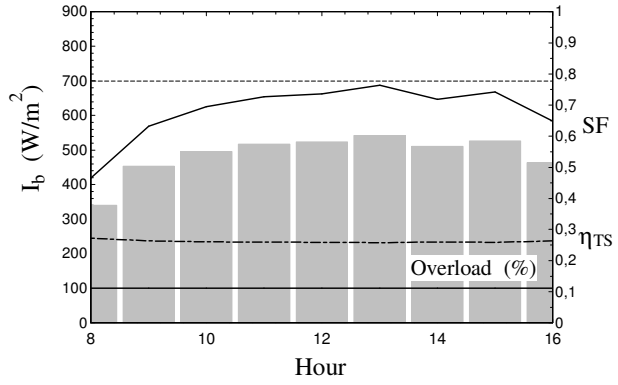


*Fig. 13. Daily radiation and calculated performance (Sede-Boqer, Negev desert; January 10th)*

*Table 4. Daily-averaged system performance for different reference days in (Sede-Boqer, Negev desert, 2007)*

| Ref. Day | $\eta_{TS}$ | SF | W, kWh |
|---|---|---|---|
| Jan 10th | 0,261 | 0,681 | 883 |
| May 19th | 0,250 | 0,902 | 1375 |
| July 8th | 0,247 | 0,946 | 1556 |
| July 17th | 0,2564 | 0,800 | 1294 |

*Table 5. Monthly system performance (Sede-Boqer, Negev desert)*

| Ref. Day | h | $\eta_{TS}$ | SF | W, kWh |
|---|---|---|---|---|
| January | 8-16 | 0,272 | 0,4748 | 23541 |
| January | 10-15 | 0,267 | 0,517 | 17165 |
| April | 7-18 | 0,272 | 0,619 | 36020 |
| April* | 7-18 | 0,252 | 0,731 | 28960 |
| July | 6-18 | 0,255 | 0,800 | 42630 |
| July | 7-17 | 0,253 | 0,854 | 36550 |

* Shutoff on days no. 2,9,14,15,25,26

## 6. Exergy analysis

An exergy analysis of the powerplant has been performed, in order to assess the exergy destruction within components and the exergy losses from the system [9], and to understand the main driving mechanisms leading to system optimization.

The calculation approach to exergy balance of power cycle is rather classic and follows traditional literature [10, 11]. The exergy inputs to the system come from (I) sun and (II) auxiliary heater. The exergy from the sun is given by:

$$\dot{E}x_{in,sun} = G_T A_C \left(1 - \frac{T_a}{T_{sun}}\right) \qquad (9)$$

where $T_{sun}$ is taken as 75% of the equivalent black-body sun temperature, in agreement with [12].

The exergy from the auxiliary heater has been taken as equivalent to the heat input (chemical exergy = Lower Calorific Value of the fuel).

The relative exergy destructions ($EXD_r$s) of power plant components (scaled to the overall exergy input) referred to the daily operation of the system are shown in figure 14 for two days, July 8th and 17th. A higher value of $EXD_{r\_coll}$ is evident on 8th July, due to the higher radiation conditions. The opposite behaviour is found for the auxiliary heater, which is turned off for a long time on sunny days.

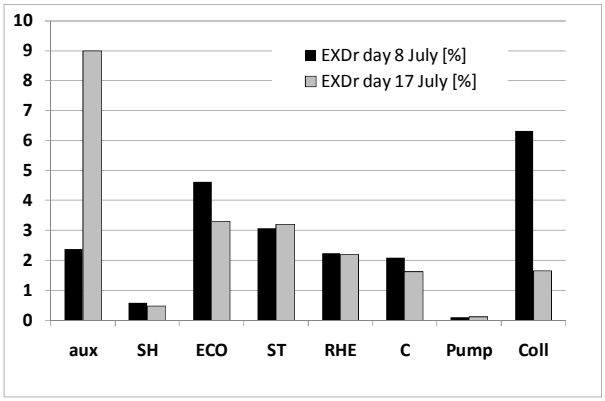


*Fig. 14. Daily relative exergy destructions of plant components*

The second relevant $EXD_r$ comes from the economiser section (ECO) of the MHE. Its contribution rises from 3.1 to 4.6% of the overall exergy input on the day with higher solar radiation (July 8th), mainly because of larger temperature difference at points 2HTF – 2 (figure 7 and schematic on figure 1). The other relevant $EXD_r$s (SH, RHE and ST) show a reduced sensitivity to solar radiation conditions.

It is interesting to observe the sum of collector's daily relative EXD and loss EXL on the two investigated days (figure 15) . The Collector Exergy Loss $EXL_{r\_coll}$ is due to the collector–environment heat dispersion. The difference between the grey and black bars in Figure 15 corresponds to the $EXD_{r\_coll}$ shown on figure 14. The largest fraction of collector's exergy inlet is lost to the environment: on the day with higher irradiation it is about 89%, whereas in the day with lower radiation it rises to 96%, showing that in this day almost all the exergy input is not transferred to the HTF but is lost to the environment.

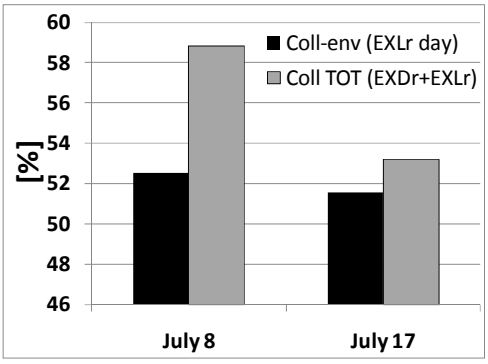


*Fig. 15. Daily relative exergy destruction and loss of solar collector*

Finally, it is interesting to observe the effect of radiation value on the hourly instantaneous absolute and relative EXDs of the main affected components (ECO, RHE and ST), as a result of off design operation (figure 16). The discussion is referred to July 8$^{th}$ only (a similar behaviour is observed on July 17$^{th}$). When the radiation is below the design value ($I_b$ < 700 W/m$^2$), the components EXDs remain unchanged, whereas they increase when $I_b$ > 700 W/m$^2$ (high-radiation off design). The ECO shows the largest increase, as a result of higher temperature difference ($T_{2HTF}$ – $T_2$ ) under off-design.

Also the RHE and ST show a relevant increase in their EXD when $I_b$ > 700 W/m$^2$, essentially because of the system flow rate control, which provides an increase in $m_{HTF}$ and $m_{WF}$, and changes significantly the temperature diagrams in the heat exchangers, as discussed at point 4.4 and shown on figure 9.

## Conclusions

A complete model for the simulation of a solar thermodynamic energy conversion system has been presented.

The advantage of a supercritical cycle has been confirmed, and the selection of the correct working fluid for the design conditions has been shown to be a key factor.

In order to allow satisfactory operation with low radiation, the system was assisted with a fuel burner. At over-design radiation conditions, the system was operated with increased flow rate and decreased efficiency. The correct selection of the design conditions, in terms of radiation, affects the Solar Fraction and the long-term system performance.

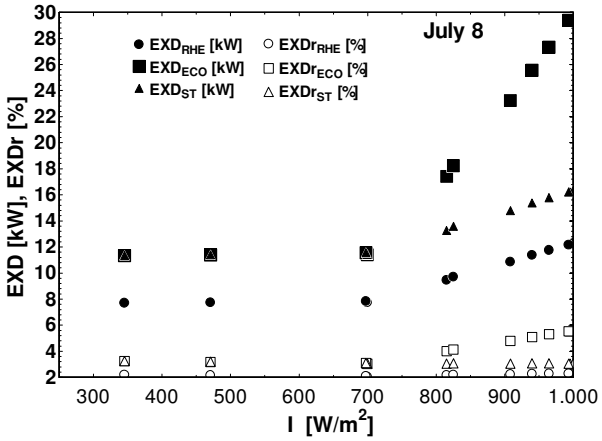


*Fig. 16. Absolute and Relative exergy destructions; ECO, RHE, ST; variable radiation (off-design)*

Off-design operation included models for the collector efficiency and heat exchanger effectiveness.

The simulations have shown that a high value of solar fraction can be achieved over a long period of the year, and that the situation can be further improved considering plant shutoff on specific days when radiation is clearly inadequate.

The exergy analysis has shown that the highest exergy destructions come from collector, ECO, RHE and ST in days of high radiation; whereas in days of low radiation the auxiliary heater plays a dominant role in the system exergy destruction. Off-design operation at high radiation conditions leads to a consistent increase of the ECO, RHE and ST exergy destructions.

## Acknowledgments

Adi Lifshitz performed part of this work during a mobility in the frame of a student cooperation agreement between University of Firenze and Tel Aviv University. The supervision of Prof. A. Kribus and Mr. A. Genani is gratefully acknowledged.

## List of symbols

$c_p$ Constant-pressure specific heat, kJ/(kgK)
$DT_{CE}$ Cold End Temp. difference (MHE),°C
$DT_{HE}$ Hot End Temperature difference (MHE),°C
$DT_{LM}$ Log-Mean Temp. difference (MHE),°C
$DT_P$ Pinch Temperature difference (MHE),°C
ECO Economizer
EVA Evaporator
EXD Exergy Destruction
EXL Exergy Loss
$I_b$ Direct radiation incident to collector aperture, W/m$^2$
m Mass flow rate, kg/s
p Pressure, kPa
Q Heat rate, kW
T Temperature, °C
U Overall heat transfer coefficient, W/(m$^2$°C)
ε Effectiveness (RHE, MHE)
η Efficiency

**Subscripts:**

abs absorber
aux auxiliary heater
c cycle
cOpt cycle, optimal (maximum condition)
C Condenser
coll Collector
D Design
day Daily value
EE End of Economizer
HTF Heat Transfer Fluid (primary circuit)
M Maximum
MHE Main Heat Exchanger
r Relative (referred to overall exergy input)
RHE Regenerative Heat Exchanger
SH Super-Heater
ST Steam Turbine
thO Overall Thermal
TS Total System
WF Working Fluid (secondary circuit)

## References

[1] Odeh,. S. D., 2003, "Unified model of solar thermal electric generation systems", Renewable Energy, 28, 755-767.

[2] ARCHIMEDE - ENEA Grande Progetto Solare Termodinamico. http://www.enea.it/com/solar/index.html

[3] Mills, D., 2004, Advances in solar thermal electricity technology, Solar Energy, 76, 19-31.

[4] Camacho, E., Berenguel, M., Rubio, F.R., 1997, *Advanced Control of Solar Plants*, Springer-Verlag, London.

[5] http://www.solel.com/products/pgeneration/ls2/

[6] Schuster, A., Karellas, S. Kakaras, E., Spliethoff, H., 2009, Energetic and economic investigation of Organic Rankine Cycle applications, Applied Thermal Engineering, 29, 8-9, 1809-181

[7] http://www.therminol.com/pages/products/vp-1.asp

[8] Cengel, Y.A., Bowles, 2002, Thermodynamics and Heat Transfer, McGraw-Hill.

[9] Bejan, A., Tsatsaronis, G., Moran, M., 1996, *Thermal Design and Optimization*, Wiley Interscience, New York.

[10] A. Bejan, 1982, *Entropy generation through heat and fluid flow*, John Wiley & Sons inc.

[11] Kotas, T.J., 1985, *The Exergy Method of Thermal Plant Analysis*, Butterworths.

[12] S. Farahat, F. Sarhaddi, H. Ajam, 2009, Exergetic optimization of flat plate solar collector, Renewable Energy, 34, 4 1169-1174.